Materials Research. 2012; 15(6): 848-858
DOI: 10.1590/S1516-14392012005000107

Three Dimensional Mathematical Model of the Iron Ore Sintering Process Based on Multiphase Theory

Jose Adilson de Castro [a,b]*, ***Yasushi Sazaki*** [b], ***Jun-ichiro Yagi*** [c]

[a]*Programa de Pós-graduação em Engenharia Metalurgica – PPGEM, Universidade Federal Fluminense – UFF, Av. dos Trabalhadores, 420, CEP 27255-125, Volta Redondam, RJ, Brazil*
[b]*Environmental Metallurgy Laboratory, Graduate Institute of Ferrous Technology, Pohang University of Science and Technology, San 31, Hyojay-Dong, Nam-Gu, Pohang, 790-784, South Korea*
[c]*Emeritus professor at Tohoku University-Sendai, Japan*

Received: February 1, 2012; Revised: May 14, 2012

In the integrated steel industries the sintering process plays an important role furnishing raw material to the blast furnace. In this work, a computational simulation of the sinter process is developed that is able to predict the most important phenomena within the sintering bed. The model is based on the multi phase concept with multiple components described by conservation equations of each component coupled with the momentum, chemical reactions and heat transfer. The model validation was carried out comparing the model predictions with averaged industrial data and local temperature measurements within the sinter strand. The model predictions presented good agreement with the averaged values measured on the industrial sinter process.

Keywords: *sintering, modeling, simulation, multiphase flow*

1. Introduction

The sintering process plays important role in the integrated route of producing hot metal in the steel industry furnishing high quality of raw materials for the subsequent production of pig iron on the blast furnace reduction process. The process is complex and involves various physical and chemical phenomena such as heat, mass and momentum transfer coupled with chemical reactions[1-3]. These phenomena take place simultaneously increasing considerably the complexity of process analysis. The raw materials used in the iron ore sintering process are furnished by several sources, from iron ore(mining sinter feed) to dust recycling within the steelworks and addition of slag agents for blast furnace and selected materials to enhance the sinter product quality, namely reactivity and mechanical strength, which plays crucial role on the blast furnace performance and reducing agent and energy consumption in the subsequent processes for steel production. In the sintering machine operation, the combustion of the solid fuels(coke breeze or anthracite) begins at the top of the layers, and as it moves, a relative narrow band of ignition zone moves downward through the bed, that can be strongly affected by the quality of the raw materials[4-9]. Several chemical reactions and phase transformations are affected, not only due to the heat front changes, but also due to modifications of local gas composition and initial melting temperatures of the mixture of raw materials. When local temperature and composition of the solids is reached, mostly the phase transformations are driven by heat supply and diffusion that take place within the particles bed with the mechanism of liquid formation playing the major role. The materials partially melt down when the local temperature reaches the melting temperature and as it moves, the contact with cold gas promotes the re-solidification and thus, the particle agglomeration forms a continuous porous sinter cake. The final sinter cake properties are strongly dependent upon the thermal cycle, initial raw materials chemical composition and thermophysical properties developed during sintering. In this paper, it is proposed a mathematical model to simulate the phenomena taking place within the sinter machine in the industrial production of sinter to the blast furnace. Figure 1 shows an schematic view of the process flow. The focus of this paper is the sinter strand where most of the phenomena which determines the final properties of the sinter product is developed. One of the most important parameter is the size distribution which influences strongly the sinter performance within the blast furnace. Previous models addressed the sintering phenomena[1,2,4,5] and mathematical models to predict the final size distribution of the sinter have been proposed[6], however, these models did not considered detailed kinetics of the sintering phenomena, which strongly affect the final size distribution[6,7]. Kasai et al[7] investigated the influence of the sinter structure into the macroscopic sinter properties. A detailed explanation of the sintering mechanism and particles interaction was provide in order to clarify the bonding forces responsible for the sinter structure and strength. At the present days, the reduction of CO_2 emissions has become an urgent issue in the steel industry as countermeasure for greenhouse emissions[3]. It is estimated that nearly 60% of the steel industry emissions are attributed to the pig iron production operation units,

*E-mail: adilson@metal.eeimvr.uff.br

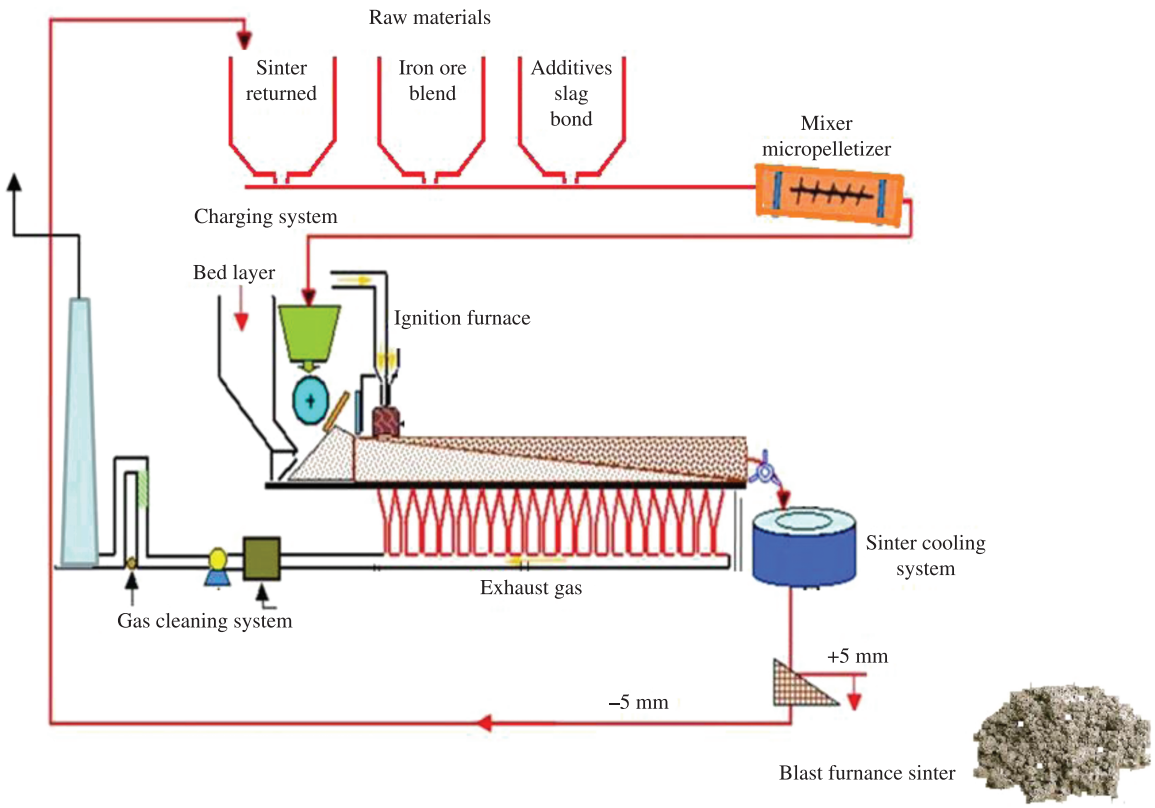

Figure 1. Schematic view for iron ore sintering process.

which includes sintering and blast furnace processes, and only the sintering process represents around 20% of this amount[1,5]. Therefore, sintering and blast furnace processes offer good opportunities to decrease the CO_2 emissions since mall decreasing of the coke breeze consumption and bonding agent used in iron ore sintering process could decisively contribute to decrease the environmental load of the steelmaking industry. Many efforts have been made to make the process cleaner and environmentally acceptable[3,8,9]. However, the process is complex and only comprehensive models can treat the phenomena and accurately quantify the impact of new technologies or design feasible operational conditions depending on the available raw materials resources. In the present work, a three dimensional mathematical model of the sinter strand is developed based on the multiphase multi-component concept and detailed interactions between the gas and solid phases are formulated. The model treats the sinter bed as a mixture of materials and gas, as presented in Figure 2 and simultaneously momentum, energy and mass transfer occur due to physical and chemical interactions. Figure 3 shows the c considered in this model. 3. Thus, the main features of the model can be summarized as follows: a) dynamic interaction of the gas mixture with the solids; b) overall heat transfer of all phases which accounts for convection and radiation phenomena; c) kinetics of vaporization and condensation of water; d) decomposition of carbonates; e) reduction and oxidation of the iron bearing materials; f) coke combustion and gasification; g) volatile matter evolution; h) shrinkage of the packed bed; h) partial melt and re-solidification of the solids and i) phase changes to form alumina-calcium-silicates. This model differs significantly from the former ones due to the concept of multiple and coupled phenomena treatment, three -dimensional treatment of the sinter strand and detailed mechanism of chemical reactions involved in the process[1,2,4,5]. Therefore, this formulation represent an advance in the task of constructing a comprehensive mathematical model of the iron ore sinter process able to consider detailed phenomena that take place in the industrial operation. In the following sections the model features are detailed and afterwards model validation on an industrial sinter machine are presented.

2. Modeling

2.1. *Model concept and assumptions*

A method for modeling the sintering process of an industrial strand machine is proposed based on multiphase, multi-component transport equations of momentum, mass and energy for gas, solid and liquid phases taking into account the local phenomena of porous sinter formation, as schematically shown in Figure 2. The model considers the phases interacting simultaneously and the chemical species of each phase is calculated based on the chemical species conservation equations. The model concept and

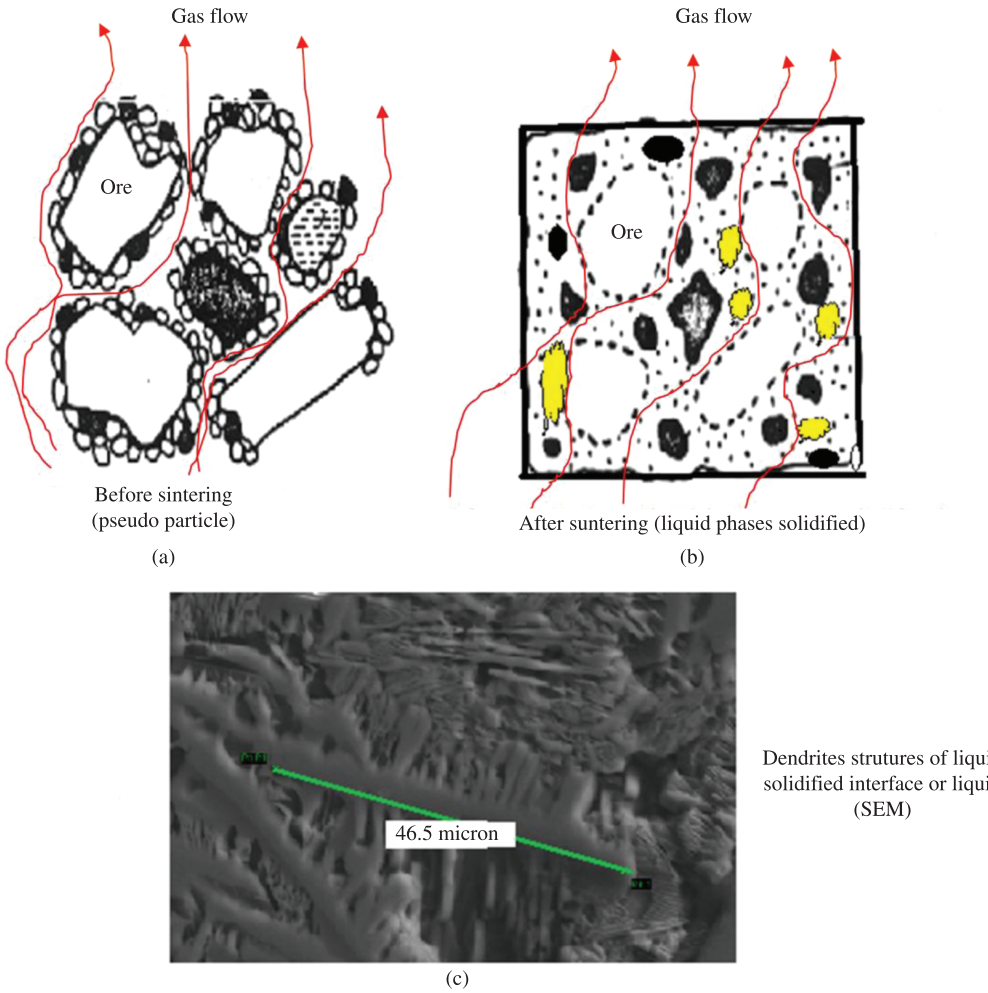

Figure 2. Gas flow heat transfer and phase evolution during the iron ore sintering.

phase interactions are shown in Figure 3. In Figure 3 the arrows shows the phases considered in the model interacting with one another. At this point, it is worthy to mention that accurate descriptions of rate exchange for momentum, energy and chemical reactions is essential to the whole accuracy of the model. The chemical species are individually taken into account by solving the transport equation of each chemical species of the gas and solid phases. The solid phase accounts for the mixture of iron ore sinter feed, fine sinter(returned fine sinter), coke breeze(or other solid fuel), scales(fines from steel plant), fluxes and limestone. The liquid phase is composed of melted and formed components in the liquid phase[10-20]. The re-solidified phase comprises the liquids re-solidified and phases formed during the re-solidification process and strongly depends on the local liquid composition and heat exchange. The final sinter cake will be formed by a mixture of these materials and its quality will depend upon the final compositions and volume fractions of each of these materials and their distribution within the mosaic sinter structure. In the present model it is assumed that the liquid phase formed will move together with the remaining solid phase due to the viscosity and considering that the liquid are formed attached on the surface of the unmelted particles, thus, equations for momentum transfer and enthalpy of the solids will account for this mixture of viscous liquid and solid materials. In the present model, the temperature-composition dependent thermophysical properties are assumed to obeys the mixture rule to take into account the individual phase properties pondered by their phase volume fractions[8,11,13,14]. The equations for momentum, energy and chemical species are convective-diffusive type equations with source and sink accounting for the external or interphase interactions phenomena, taking into account the transient, convective, conductive and source terms, as follows[1,2,8,13,14]

Momentum:

$$\frac{\partial\left(\rho_i \varepsilon_i u_{i,j}\right)}{\partial t}+\frac{\partial\left(\rho_i \varepsilon_i u_{i,k} u_{i,j}\right)}{\partial x_k}=\frac{\partial}{\partial x_k}\left(\mu_i \frac{\partial u_{i,j}}{\partial x_k}\right)-\frac{\partial P_i}{\partial x_j}-F_j^{i-l} \qquad (1)$$

Continuity:

$$\frac{\partial\left(\rho_i \xi_i\right)}{\partial t}+\frac{\partial\left(\rho_i \xi_i u_{i,k}\right)}{\partial x_k}=\sum_{m=1}^{Nreacts} M_n r_m \qquad (2)$$

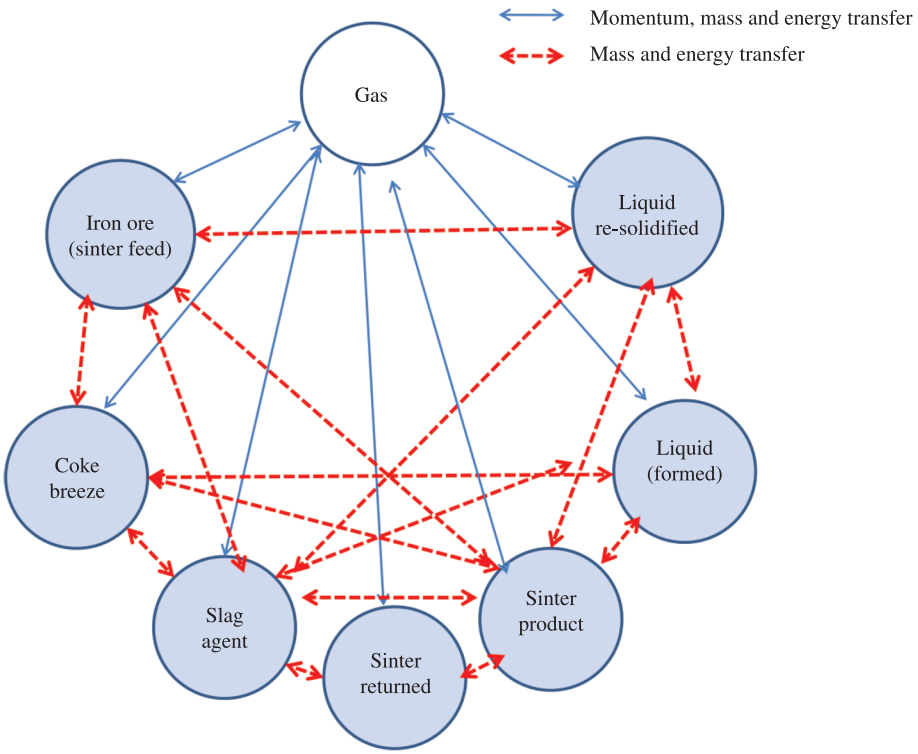

Figure 3. Multiphase momentum, heat and mass interactions considered in the present model.

Enthalpy balance:

$$\frac{\partial(\rho_i \varepsilon_i h_i)}{\partial t} + \frac{\partial(\rho_i \varepsilon_i u_{i,k} h_i)}{\partial x_k} = \frac{\partial}{\partial x_k}\left(\frac{k_i}{C_{pi}}\frac{\partial h_i}{\partial x_k}\right) + E^{i-l} + \sum_{m=1}^{Nreacts} \Delta h_m r_m \quad (3)$$

The chemical species are individually considered within the phase, for gas, or components of the solid or liquid phases, as presented in Equations 4.

$$\frac{\partial(\rho_i \varepsilon_i \varphi_n)}{\partial t} + \frac{\partial(\rho_i \varepsilon_i u_{i,k} \varphi_n)}{\partial x_k} = \frac{\partial}{\partial x_k}\left(D_n^{eff}\frac{\partial \varphi_n}{\partial x_k}\right) + \sum_{m=1}^{Nreacts} M_n r_m \quad (4)$$

Where indexes ***i*** and ***l*** represent the phases, ***j*** and ***k*** are the indexes for coordinates component direction ***n*** is chemical species and m the indicator of the reactions, M is the molecular weight of the species, ***P*** is phase pressure, ***F*** is component of momentum interactions among the phases and ***r*** is the rate of chemical reactions. ρ,ε,Cp, k and Δh are phase density, volume fractions, heat capacity, heat conductivity and heat due to chemical reactions, respectively. The quantity E^{i-l} is the heat transfer among the phases and accounts for convective and radiation heat transfer, since conductive heat transfer is include in Equations 3. The gas -solids momentum interactions are represented by F^{i-l}. The model equations are completed with suitable correlations for the thermophysical properties of the phases, rate equations for the source terms and the initial and boundary conditions representing the sintering process. The chemical species considered in this model are presented in Table 1. As already mention, the chemical reactions and the phase transformations occurring within the sinter bed play important role on the local temperature and composition and hence at the final sinter product. This model considers the set of chemical and phase transformations listed in Table 2 and 3. Within the bed the model considers solid combustion, carbonates decomposition, iron ore reduction and re-oxidation, melting and re-solidification, water vaporization and liquid phases formation. The kinetics of these transformations depends on the local temperature and composition. The rate equations for the chemical reactions considered in this model where obtained from literature[8,11-14].

2.2. *Boundary and initial conditions*

The model formulation represented by Equations 1-4 are completed with the initial and boundary conditions. The computational domain is defined by the region of the sinter strand for the case of the industrial scale process simulation and the equations are solved considering steady state conditions, therefore the first terms on the left of the equations are set to zero and the initial conditions are regard as initial tentative values for the numerical interactions. Regarding to the boundary conditions for the solid phase, the composition, initial and inlet particle diameters, charging particle and volume fractions distributions and moisture content are specified at the charging position of the strand. The chemical compositions of the raw materials used in this study as inlet conditions is presented in Table 4. The outlet boundary condition for the solid phase is assumed fully developed flow and no sleep condition is assumed at the sinter strand. The other boundaries such as lateral and bed

Table 1. Phases and chemical species considered in the model.

Equations of the gas phase			
Gas	Momentum	$u_{1,g}$, $u_{2,g}$,$u_{3,g}$, P_g, ε_g	
	Energy	h_g	
	Chemical species	N_2, O_2, CO,CO_2, H_2O, H_2, SiO, SO_2, CH_4	
Equations of the solid phase			
Solid	Momentum	$u_{1,s}$, $u_{2,s}$,$u_{3,s}$, P_s, ε_s	
	Energy	h_s	
	Chemical species	Coke breeze	C,Volatiles, H_2O, Al_2O_3, SiO_2, MnO, MgO, CaO, FeS, P_2O_5, K_2O, Na_2O, S_2
		Iron ore (sinter feed)	Fe_2O_3, Fe_3O_4, FeO, Fe, H_2O, Al_2O_3, SiO_2, MnO, MgO, CaO, FeS, P_2O_5, K_2O, Na_2O
		Return Sinter (bed material)	Fe_2O_3, Fe_3O_4, FeO, Fe, H_2O, Al_2O_3, SiO_2, MnO, MgO, CaO, FeS, P_2O_5, K_2O, Na_2O
		Solidified materials	Fe_2O_3, Fe_3O_4, FeO, Fe, H_2O, Al_2O_3, SiO_2, MnO, MgO, CaO, FeS, P_2O_5, K_2O, Na_2O, $Ca_2Fe_3O_5$, Al_2MgO_4
		Fluxing agent	(MgOCaO)CO_3, CaO, H_2O, Al_2O_3, SiO_2, MnO, MgO, TiO_2
		Sinter cake	Fe_2O_3, Fe_3O_4, FeO, Fe, H_2O, Al_2O_3, SiO_2, MnO, MgO, CaO, FeS, P_2O_5, K_2O, Na_2O, $Ca_2Fe_3O_5$, Al_2MgO_4
Liquid	Chemical Species	Intrabed liquid	Fe_2O_3, Fe_3O_4, FeO, Fe, H_2O, Al_2O_3, SiO_2, MnO, MgO, CaO, FeS, P_2O_5, K_2O, Na_2O, $Ca_2Fe_3O_5$, Al_2MgO_4

Total of 118 partial differential equations numerically solved using the finite volume technique.

Table 2. Chemical reactions considered in the model.

Solid fuels reactions	
$C(i)+O_2(g)\rightarrow CO_2(g)$ (full combustion)	$C(i)+\frac{1}{2}O_2(g)\rightarrow CO(g)$ (partial combustion)
$C(i)+CO_2(g)\rightarrow 2CO(g)$	$C(i)+H_2O(g)\rightarrow CO(g)+H_2(g)$
$\text{volatiles(i)}+\alpha_1 O_2 \rightarrow \alpha_2 CO_2(g)+\alpha_3 H_2O(g)+\alpha_4 N_2(g)$	
$\text{volatiles(i)}+\alpha_5 CO_2(g)\rightarrow \alpha_6 CO(g)+\alpha_7 H_2(g)+\alpha_8 N_2(g)$ - (I = coke breeze, anthracite and scale)	
Note: the stoichiometric coefficients depends on the elemental analysis of the solid fuel	
Carbonates decomposition	
$CaCO_3\rightarrow CaO+CO_2(g)$	$MgCO_3\rightarrow MgO+CO_2(g)$
Iron oxides reduction/Re-oxidation	
$Fe_2O_3(i)+CO/H_2(g)\rightarrow Fe_3O_4(i)+CO_2/H_2O(g)$	(i = iron ore, return sinter and scale)
$\frac{w}{4w-3}Fe_3O_4(i)+CO/H_2(g)\rightarrow \frac{3}{4w-3}Fe_wO\ (i)+CO_2/H_2O(g)$	(i = iron ore, return sinter and scale)
$Fe_wO\ (i)+CO/H_2(g)\rightarrow wFe(i)+CO_2/H_2O(g)$	(i = iron ore, return sinter and scale)
$wFe(i)+\frac{1}{2}O_2(g)\rightarrow Fe_wO\ (i)$	(i = iron ore, return sinter and scale)
$\frac{3}{4w-3}Fe_wO\ (i)+\frac{1}{2}O_2(g)\rightarrow \frac{w}{4w-3}Fe_3O_4(i)$	(i = iron ore, return sinter and scale)
$2Fe_3O_4(i)+\frac{1}{2}O_2(g)\rightarrow 3Fe_2O_3(i)$	(i = iron ore, return sinter and scale)
Water vaporization/condensation/gas equilibrium	
$H_2O(i)\ \leftrightarrow\ H_2O(g)$	(i = iron ore, return sinter and scale)
$CO_2(g)+H_2(g)\leftrightarrow CO(g)+H_2O(g)$ (gas equilibrium)	$CO+\frac{1}{2}O_2\rightarrow CO_2$ $H_2+\frac{1}{2}O_2\rightarrow H_2O$

Table 3. Liquid formation and bonding phases considered in the model.

$2\,CaO(i)+SiO_2(i)\rightarrow Ca_2SiO_4(i)\rightarrow Ca_2SiO_4(l)\rightarrow Ca_2SiO_4(ls)$	$Fe_xO_y(i)\rightarrow Fe_xO_y(l)\rightarrow Fe_xO_y(ls)$
$2\,CaO(l)+SiO_2(l)\rightarrow Ca_2SiO_4(l)\rightarrow Ca_2SiO_4(ls)$	$Al_2O_3(i)\rightarrow Al_2O_3(l)\rightarrow Al_2O_3(ls)$
$CaO(l)+SiO_2(l)\rightarrow CaSiO_3(l)\rightarrow CaSiO_3(ls)$	$MgO(i)\rightarrow MgO(l)\rightarrow MgO(ls)$
$2\,CaO(i)+Fe_2O_3(i)\rightarrow Ca_2Fe_2O_5(i)\rightarrow Ca_2Fe_2O_5(l)\rightarrow Ca_2Fe_2O_5(ls)$	$CaO(i)\rightarrow CaO(l)\rightarrow CaO(ls)$
$2\,CaO(l)+Fe_2O_3(l)\rightarrow Ca_2Fe_2O_5(l)\rightarrow Ca_2Fe_2O_5(ls)$	$SiO_2(i)\rightarrow SiO_2(l)\rightarrow SiO_2(ls)$
$CaO(l)+Fe_2O_3(l)\rightarrow CaFe_2O_4(l)\rightarrow CaFe_2O_4(ls)$	$MnO(i)\rightarrow MnO(l)\rightarrow MnO(ls)$

(i: iron ore, return sinter, flux and scale ; l: liquid; ls: liquid solidified).

surface are assumed zero velocities components gradient. For the energy balance equations convective and radiation coefficients are assumed for each of these surfaces(assumed 100 W.m^{-2} K and emissivity 0.8 for gas and solid phases). The gas inlet and outlet flow rates are determined by the pressure drop specified for each wind box and it is calculated interactively by considering simultaneously the mass balance and pressure drop of each wind box. The gas inlet temperature is specified at the surface of the bed and the outlet temperature are calculate by assuming fully developed flow. As for the chemical species for the gas phase, specified values on the surface of the sinter bed are assumed and similarly the solid phase the outlet values are calculated by using fully developed flowing conditions at the bottom of the bed. The strand velocity and dimensions(width, length and bed height) are given as input data for each machine. The charging system distribute the materials in the strand and some segregation may occurs, however due to lake of information and sake of simplicity it was not taken into consideration for the calculations carried out in this investigation.

2.3. *Numerical features*

The multiphase model is composed of a set of partial differential equations that can only be solved by numerical methods due to their nonlinearities on the boundary conditions and source terms. In this work, the set of differential equations described above is discredited by using the finite volume method[15] and the resulting set of algebraic equations are solved by the iterative procedure using the line by line method combined with the tri-diagonal matrix solver algorithm[15]. In this paper, the numerical grid used to simulate the industrial strand of the sinter machine was discretized based on the Cartesian coordinate system with 10 × 140 × 12 = 16800 control volumes, assumed suitable for the calculations after continuous grid refinement procedure to assure solutions independence of the control volume size. The numerical convergence was accepted for tolerance of the order of 10^{-6} for the velocity and temperature fields, meanwhile, for the chemical species the overall mass balance was accepted less than 1% for all chemical species calculated.

2.4. *Source terms*

The momentum transfer between the solid and gas are modeled based on the modified Ergun's equation, which takes into account the local soft-melting behavior of the raw materials with the volume fraction and effective diameters modified by the soft-melting data, as follows[4,11-14]

$$F_j^{g-s}=\left[1.75\rho_g+\frac{150\mu_g}{\left|\vec{U}_g-\vec{U}_s\right|\left(\frac{\varepsilon_s}{d_s\phi_s}\right)}\right]\left(\frac{\varepsilon_s}{(1-\varepsilon_s)^3\,d_s\phi_s}\right)\left|\vec{U}_g-\vec{U}_s\right|\left(u_{g,j}-u_{s,j}\right) \quad (5)$$

The overall heat transfer coefficient between the gas and the packed bed[11-13] is given by Equation 6.

$$E^{g-s}=\frac{6\varepsilon_s}{d_s\phi_s}\frac{k_g}{(d_s\phi_s)}\left[2+0.39\left(\mathrm{Re}_{g-s}\right)^{1/2}\left(\mathrm{Pr}_g\right)^{1/3}\right]\left(T_g-T_s\right) \quad (6)$$

As shown in Equation 6, the gas-solid system inter-phase heat transfer is given by the product of the overall effective heat transfer coefficient, the interfacial area and the average temperature differences of the bed and gas phase. The parameters of the sinter bed ε_s d_s and φ_s are temperature dependent and account for the effective volume fraction, particle diameter and shape factor, respectively, which strongly affect the momentum and energy transfer on the soft-melting zone. The solid diameters and shape factors are given as raw materials properties from the harmonic average of the particle size distributions. In the present model these parameters are calculated by using soft-melting experimental data for the raw materials used[8,16-20], as presented by Equations 7-9.

$$\varepsilon_i=1-\left(0.403\left[100d_i\right]^{0.14}\right)\left(1-MAX\left(0,\ MIN\left(1,\left(\frac{T_s-T_{im}}{\Delta T_m}\right)\right)\right)\frac{S_m}{100}\right) \quad (7)$$

$$\varepsilon_s=\sum\varepsilon_i+\varepsilon_l+\varepsilon_{ls} \quad (8)$$

$$d_s=d_{initial}+\left(d_{final}-d_{initial}\right)\left(\frac{\varepsilon_l+\varepsilon_{ls}}{\varepsilon_s}\right)^3 \quad (9)$$

Where *i* stands for iron ore sinter feed, retuned sinter, solid fuels, fluxes and scales on the sintering mixture charged on the sinter bed, *l* and *ls* are the liquid and solid bridges volume fractions formed during sintering phenomena. The average size of the sintering structure are given by Equations 9 with the parameters $d_{initial}$ and d_{final} representing the average particle size of the quasi particles charged in

Table 4. Chemical compositions of the raw materials used as input for the model.

Iron and flux sources(%mass)									
	C	**CLW**	**Fe_2O_3**	**Fe**	**H_2O**	**SiO_2**	**Al_2O_3**	**MgO**	**CaO**
Iron ore sinter feed	-	2.4	92.0	-	-	3.5	1.3	0.4	0.4
Returned sinter (bed formation)	-	-	87.4	-	1.3	3.2	1.2	1.3	5.6
Fluxes (slaging agent)	-	-	-	-	0.8	2.5	1.4	13 ($MgCO_3$)	82 ($CaCO_3$)
Solid fuel(% mass)									
	C	**VM**	**Fe_2O_3**	**Fe**	**H_2O**	**SiO_2**	**Al_2O_3**	**MgO**	**CaO**
Coke breeze	86.9	1.4	-	-	4.3	4.1	3.0	0.1	0.2
Scale	31.9	3.1	10.8	35.5	5.8	6.6	4.1	0.4	1.7

VM: Volatile mater - H_2O : Humidity CWL: Calcination weight loss.

Table 5. Global parameters validation.

	Production (t/h)	**Productivity ($t/m^2/day$)**	**Gas flow (Nm^3/min)**	**Fuel (kg/t)**	**Sinter feed (kg/t)**	**Return sinter (kg/t)**	**Fluxes (kg/t)**	**Suction depression (kPa)**
Process	827.3	41.2	14565.5	45.8	573.3	323.5	133.1	14.1
Model	830.5	41.4	14451.3	46.5	573.8	324.5	133.8	13.8
Error(%)	0.4	0.1	0.8	1.5	0.1	0.7	0.5	2.1

Other parameters

Initial pseudo particle diameter (mm) (input data) $d_{initial}$ in Equation 9	Final particle diameter (mm) (calculated) d_{final} in Equation 9	Coke breeze average particle diameter (mm) (input data)	Iron ore particle diameter (mm) (input data)	Limestone particle diameter(mm) (input data)	Liquid solidified (%) (calculated)
7.5	40	3.2	4.3	1.5	65
Initial temperature - (T_{im},) in Equations 7 (°C)		Melting interval (ΔT_m) in Equations 7 (°C)		Shrinkage (S_m) in Equations 7 (%)	
1055		215		35	

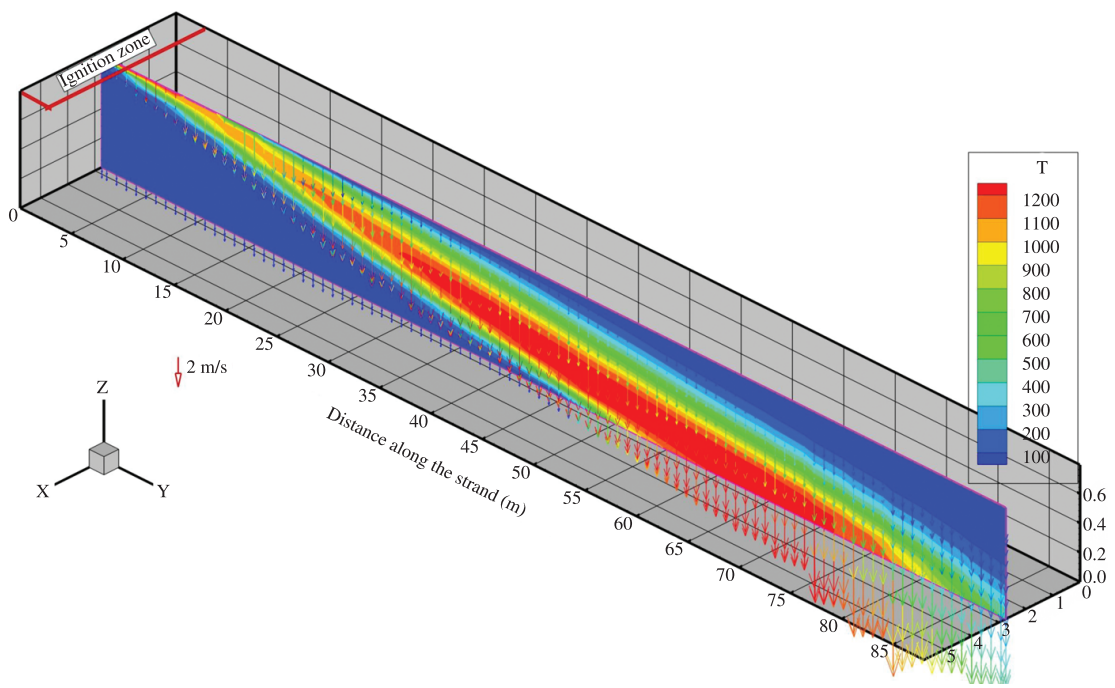

Figure 4. Calculated gas flow distribution vector and temperature pattern for a vertical plane on the sinter bed (°C).

the bed and the particle size for complete sintering product[2]. In the present model these parameters are given for each sintering mixture with their own soft-melting data. As softening-meting data the model uses the parameters T_{im}, ΔT_m and S_m representing the initial melting temperature, meting temperature interval and percentage of shrinkage. This parameters are obtained from the pressure *vs* temperature curve obtained from the softening-melting experiment[16-20].

3. Results and Discussions

In order to validate the implemented simulation numerical code an industrial operating sinter process was monitored in order to select the input data and model validation to demonstrate the model accuracy. The model validation was carried out by monitoring the sinter bed temperature into 3 distinct height of the bed by inserting encapsulated thermocouples and recording the temperature measurements along the bed motion. The data used in this calculations were assumed the averaged values of 6 hours of uninterrupted operation(corresponding to a complete turn of continuous operation). In this interval 3 runs of temperature measurement were carried out and the averaged values of the temperatures where used to compared with the numerical predictions with the input average data of strand velocity and raw materials mix of this time interval. Figure 4 shows the gas vectors velocity and temperature predictions for the middle vertical plane of the sinter strand. As can be observed, the gas velocity gradually increases as the sinter strand moves. This results is explained by the effect on the gas flow of bed permeability evolution and density changes of the gas phase due to changes in the gas temperature, pressure and composition (this model uses the ideal gas relation to account for this effects on the density). As observed, the final burn out temperature reach the position of 65 m, which correspond the wind box number 18 in the present sinter machine. Figure 5 presents the comparison of temperature predictions by the model and measured data obtained in the industrial sintering machine for the actual operation conditions. The calculated results were compared with the averaged measured data obtained by thermocouples inserted within the sinter bed on fixed positions of 75 mm, 355 mm and 725 mm within the bed and the temperatures were recorded on intervals of 10 m along the strand. As can be observed (see Table 5), the measured and predicted values are in excellent agreement, considering that the temperature are strongly effect by all the phenomena simultaneously taking place in the sinter bed such as interphase heat transfer, phase changes, momentum transfer and chemical reactions. These results indicated that the model is enough accurate to predict the industrial process of iron ore sintering. Figure 6 shows the comparison for prediction of gas composition at the outlet of the sinter bed with the measurements carried out at the wind boxes of the sinter strand. The model presents same trend of the measured values and good agreement. It is seemed that the model predictions are systematically higher than the measured values, which may be explained due to water condensation in the wind boxes. Figure 7 shows tridimensional slices of the sinter bed indicating the temperature distributions. As observed, the tridimensional nature of the process is evidenced. However, as claimed by some authors at the literature[1,2,5], when the charging system and bed permeability are strictly controlled the middle vertical is a symmetry plane and can be used for a fast estimation of the whole process. However, the process control are note tiny and some tridimensional distribution is usually observed. This model allows the treatment of these asymmetric conditions when needed.

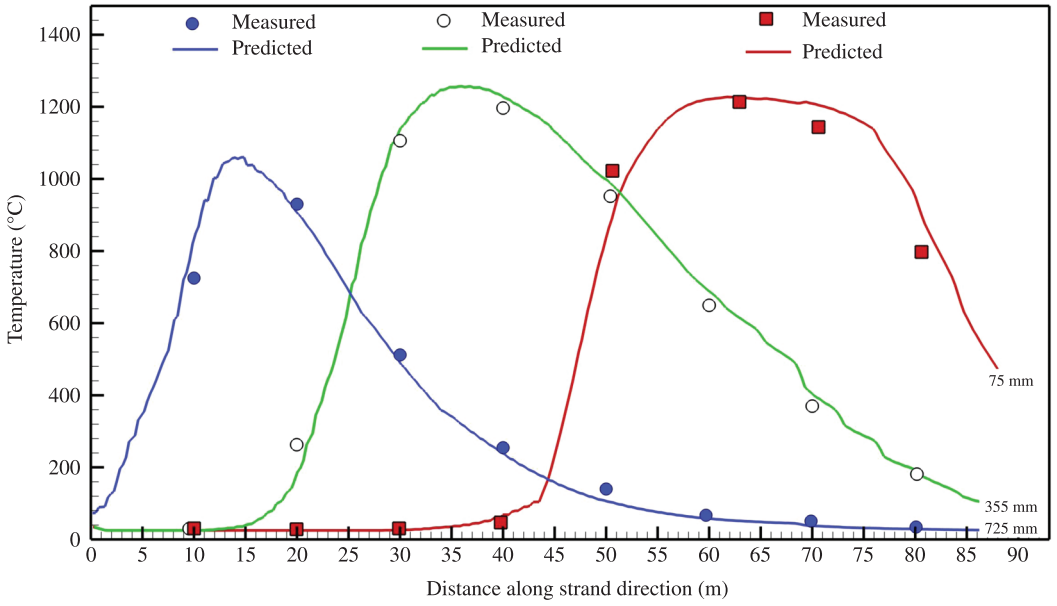

Figure 5. Model prediction and thermocouples measurements in the sinter bed (°C).

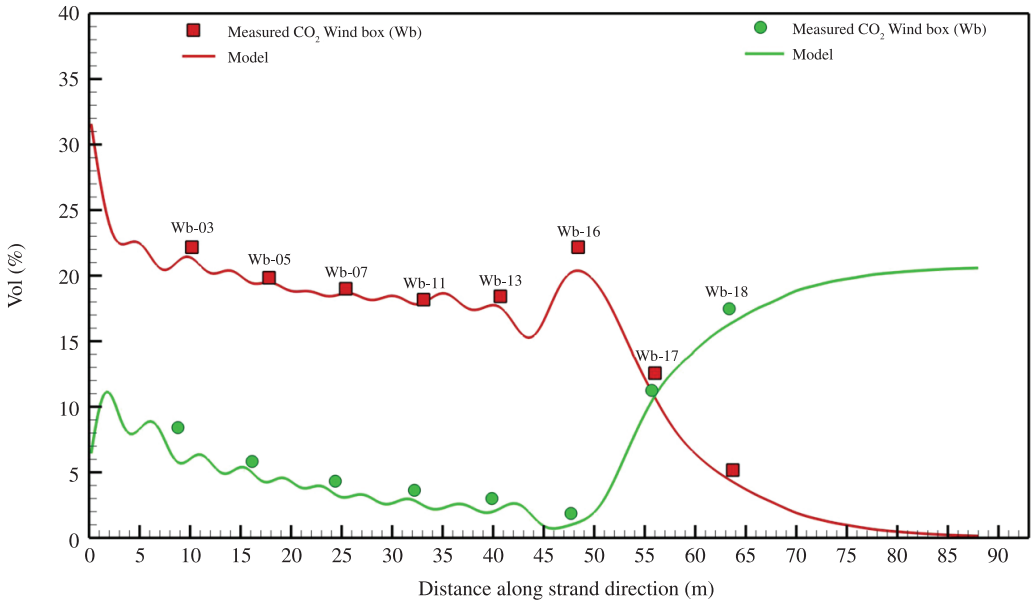

Figure 6. Gas composition measurements and model predictions for wind boxes along the strand.

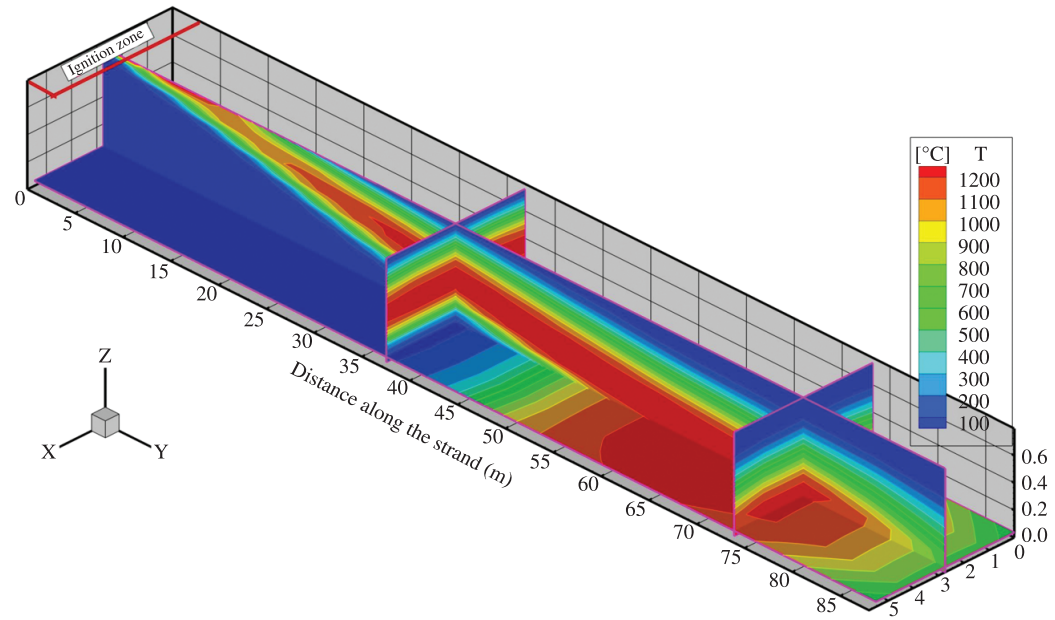

Figure 7. Three dimensional solid temperature distribution in the sinter bed (°C).

4. Conclusions

In this paper a multiphase 3D mathematical model able to simulate the process phenomena of the sinter bed of an industrial operation was presented. The model is based on transport equations of momentum, energy and chemical species coupled with chemical reaction rates, which takes into account the phase flows, heat exchange and mass transfer considering the chemical reactions and phase transformations. The model was validated by sinter bed temperature measurements obtained by inserting thermocouples into the sinter bed of the industrial sinter machine. It was demonstrated the 3D behavior of the sinter front and inner temperature distributions. The model demonstrated the capability to simulate the actual sinter operation conditions and represents useful tool to design feasible operation conditions.

Acknowledgements

This study was partially supported by CNPq - Conselho Nacional de Desenvolvimento Científico e Tecnológico and Faperj - Fundação Carlos Chagas Filho de Amparo a Pesquisa do Estado do Rio de Janeiro - Brazil.

References

1. Cumming MJ and Thurlby JA. Developments in modeling and simulation of iron ore sintering. *Ironmaking and Steelmaking.* 1990; 17:245-254.
2. Nath NK, Silva AJ and Chakraborti N. Dynamic process modeling of iron ore sintering. *Steel Research*. 1997; 68:285-292.
3. Oyama N, Iwami Y, Yamamoto T, Machida S, Yguchi T, Sato H et al. Development of secondary-fuel injection technology for energy reduction in the iron ore sintering process. *ISIJ International*. 2011; 51:913-921. http://dx.doi.org/10.2355/isijinternational.51.913
4. Yamaoka H and Kawaguchi T. Development of a 3-D sinter process mathematical simulation model. *ISIJ International*. 2005; 45:522-531. http://dx.doi.org/10.2355/isijinternational.45.522
5. Mitterlehner J, Loeffler G, Winter F, Hofbauer H, Smid H, Zwittag E et al. Modeling and simulation of heat front propagation in the iron ore sintering process. *ISIJ International*. 2004; 44:11-20. http://dx.doi.org/10.2355/isijinternational.44.11
6. Waters AG, Lister JD and Nicol SK. A mathematical model for the prediction of granule size distribution for multicomponent sinter feed. *ISIJ International*. 1989; 29:274-283. http://dx.doi.org/10.2355/isijinternational.29.274
7. Kasai E, Komarov S, Nushiro K and Nakano M. Design of Bed Structure Aiming the Control of Void Structure Formed in the Sinter Cake. *ISIJ International*. 2005; 45:538-543. http://dx.doi.org/10.2355/isijinternational.45.538
8. Castro JA, Silva AJ, Nogami H and Yagi J. Modelo matematico tridimensional multifasico da geração de dioxinas no leito de sinterização. *TMM-Tecnologia em Metalurgia e Materiais*. 2005; 2:45-49. http://dx.doi.org/10.4322/tmm.00202009
9. Kasama S, Yamamura Y and Watanabe K. Investigation on the Dioxin Emission from a commercial Sintering Plant. *ISIJ International*. 2006; 46:1014-1019. http://dx.doi.org/10.2355/isijinternational.46.1014
10. Jeon JW, Jumg SM and Sasaki Y. Formation of Calcium Ferrites under Controlled Oxygen Potentials at 1273 K. *ISIJ International*. 2010; 50:1064-1070. http://dx.doi.org/10.2355/isijinternational.50.1064
11. Castro JA, Nogami H and Yagi J. Three dimensional multiphase mathematical modeling of the blast furnace based on multifluid theory. *ISIJ International*. 2002; 42:44-52. http://dx.doi.org/10.2355/isijinternational.42.44
12. Austin PR, Nogami H, and Yagi J. A mathematical model for blast furnace reaction analysis based on the four fluid model. *ISIJ International*. 1997; 37:748-755. http://dx.doi.org/10.2355/isijinternational.37.748
13. Omori Y. *The blast furnace phenomena and modeling*. London: Elsevier Applied Science; 1987.
14. Hou P, Choi S, Yang W, Choi E and Kang H. Aplication of intraparticle combustion model for iron ore sinter bed. *Materials Science and Applications*, 2011; 2:370-380. http://dx.doi.org/10.4236/msa.2011.25048
15. Melaen MC. Calculation of fluid flows with staggered and nonstaggered curvelinear nonorthogonal grids-the theory. *Numerical Heat Transfer*. 1992; B 21:1-19.
16. Nogueira PF and Fruehan RJ. Blast furnace burden softening and melting phenomena: part III melt onset and initial microstructural transformations in pellets. *Metallurgical and Materials Transactions B.* 2006; 37B:551-558. http://dx.doi.org/10.1007/s11663-006-0038-3
17. Nogueira PF, Castro AA and Pimenta HP. High temperature properties of sinters and pellets produced with Brazilian ores. In: *Proceedings of the 4th International Congress on the Science and Technology of Ironmaking;* 2006; Osaka. Osaka; 2006. v. 1, p. 671-674.
18. Nandy, Chandra BS, Bhattacharjee D and Ghosh D. Assessment of blast furnace behaviour through softening-melting test. *Ironmaking and Steelmaking.* 2006; 33:111-119. http://dx.doi.org/10.1179/174328106X94744
19. Oyama N, Higuchi T, Machida S, Sato H, and Takeda K. Effect of high-phosphorous iron ore distribution in quasi-particle on melt fluidity and sinter bed permeability during sintering. *ISIJ International*. 2009; 49:650-658. http://dx.doi.org/10.2355/isijinternational.49.650
20. Lv X, Bai C, Deng Q, Huang X and Qiu G. Behavior of Liquid Phase Formation during Iron Ores Sintering. *ISIJ International.* 2011; 51:722-727. http://dx.doi.org/10.2355/isijinternational.51.722

Appendix 1. Nomenclature.

A: surface area, (m2 m-3)

C_p: heat capacity, (J kg^{-1} K^{-1})

d_m: solid component diameter, (m)

d_s: solid phase mean diameter, (m)

$d_{initial}$: Initial micro pellets charged , (m)

d_{final}: solid agglomerated, (m)

F_j^{i-l} : interaction force in *j* direction between *i* and *l* phases, (Nm^{-3} s^{-1})

h : enthalpy of the phase (kJ kg^{-1})

$\vec{U}_i$: phase velocity vector (I = gas and solid), (m s^{-1})

P : phase pressure (Pa)

$\mathrm{Pr}_g = \frac{C_{p,g}\mu_g}{k_g}$: Prandtl number, (-)

$\mathrm{Re}_{g-s} = \frac{\rho_g \left|\bar{U}_g - \bar{U}_s\right|}{\mu_g} d_s$: particle Reynolds number, (-)

R: gas constant, (J mol^{-1} K^{-1})

r_m : rates of chemical or phase transformations, (kmol m^{-3} s)

S_ϕ: source or sink terms for the ϕ variables, (various)

S_m : Volume shrinkage in the sintering zone (%)

x_i: spatial coordinates, (m)

t: time, (s)

T: temperature, (K)

T_{im} : initial melting temperature (K)

Greek symbols

ΔT_m : melting temperature interval of the iron ore (K)

ϕ_n: mass fraction in Equation 4, (calculated by the model), [$kg.kg^{-1}$]

φ_m: solid diameter shape factor (m=sinter feed, sinter return, limestone, fines, coke, mushy and bonding), (-)

ε_i: volume fractions (m^3 m^{-3})

ρ_i : phase density (I = gas and solid), (kg m^{-3})

μ: phase effective viscosity (Pa s)